Latin American Journal of Solids and Structures
www.lajss.org

Numerical and Experimental Study on the Formation and Dispersion Patterns of Multiple Explosively Formed Penetrators

Abstract

Three-dimensional numerical simulations and experiments were performed to examine the formation and spatial dispersion patterns of integral multiple explosively formed penetrators (MEFP) warhead with seven hemispherical liners. Numerical results had successfully described the formation process and distribution pattern of MEFP. A group of penetrators consisting of a central penetrator surrounded by 6 penetrators is formed during the formation process of MEFP and moves in the direction of aiming position. The maximum divergence angle of the surrounding penetrator group was 7.8°, and the damage area could reach 0.16 m^2 at 1.2 m. The laws of perforation dispersion patterns of MEFP were also obtained through a nonlinear fitting of the perforation information on the target at different standoffs. The terminal effects of the MEFP warhead were performed on three #45 steel targets with a dimension of 160cm × 160cm × 1.5cm at various standoffs (60, 80, and 120 cm). The simulation results were validated through penetration experiments at different standoffs. It has shown excellent agreement between simulation and experiment results.

Keywords

Multiple Explosively Formed Penetrators (MEFP); Formation; Penetration; Standoff; Dispersion pattern

Jian Feng Liu [a]
Yuan Long [b]
Chong Ji [c]
Quan Jun Xu [d]
Fu Yin Gao [e]
Chang Xiao Zhao [f]

[a] College of Field Engineering, PLA Univ. of Sci.&Tech., China
ljflccc@163.com
[b] College of Field Engineering, PLA Univ. of Sci.&Tech., China
long_yuan@sohu.com
[c] College of Field Engineering, PLA Univ. of Sci.&Tech., China
blastingcaptain@163.com
[d] College of Field Engineering, PLA Univ. of Sci.&Tech., China
[e] College of Field Engineering, PLA Univ. of Sci.&Tech., China
[f] Wuhara Ordraarrce NCO Acadeuay, PLA, China

http://dx.doi.org/10.1590/1679-78253385

Received 18.09.2016
Accepted 21.02.2017
Available online 04.03.2017

1 INTRODUCTION

Multiple explosively formed penetrator (MEFP) warhead technologies have a very promising option in the category of defeating targets such as low-flying aircraft, attacking missiles and light armors

[William et al., 2002; Bender et al., 2001]. Compared with conventional explosively formed penetrator (EFP) [Kazoo and Takenori,2013], MEFP provides a warhead that can produce a focused cluster of numerous penetrators that increases its hitting probability and killing capability [Johnson and Stryk,2006].

MEFP warhead can be categorized into combined-type, incised-type, and integral-type in accordance with its charge structure. A combined-type MEFP warhead [Zhang et al., 2012; Zhou et al.,2006] is made up of a serial of sub-charges (EFP charge) and filling material. In this mode, multiple detonators laid in an array at the back of each sub-charge are detonated. Controlling the shape and divergence angle of MEFP using the multiple detonators approach is difficult because the explosion fields formed by every sub-charge will interact with one another after initiation. For MEFP patterns with an incised-type [Long et al., 2010, 2013; Richard Fong et al.,1996], the liner is driven to pass through a cutting mechanical device. The device is designed to break up the liner and form a group of compact damage elements to achieve the desired spatial distribution pattern of penetrators. However, large mass losses and a decline in the velocity of MEFP occur because of the cut and resist of the cutting mechanical device. The integral-type MEFP warhead [Saroha et al., 2010; Bill et al., 1991] is primarily selected as a part of munition systems because the structure of the integral MEFP charge is strongly relevant with a single EFP [Wu et al., 2007] in technology and is easy to accomplish. The warhead is composed of an integral explosive with many liners and detonator placed in the back of the charge. A controlled pattern of penetrators that cover a large damage area eliminates the need for precision aiming and increases the probability of hitting the target.

In the past decades, researchers started to design and test the properties of MEFP warheads owing to the significant advantages offered by integral MEFP warheads. The U.S. Army TACOM-ARDEC Warhead Group [Richard et al., 2001, 2005] has conducted analyses and tests in integral MEFP warhead technology. Its MEFP warhead technology has been applied in many systems to attack various targets, including armors of different thicknesses, materials, and minefields. In 1999, Fraunhofer Institut für Kurzzeitdynamik Ernst Mach Institut Group [Blachel and Weimann] performed an experiment on an integral MEFP warhead against lightweight armor. The effect of multipoint initiation and initiating systems of VESF on the formation and penetration of MEFP were studied. The Group designed a double curvature liner in a MEFP warhead that can form a penetrator with a total energy of 512 J at 2 m standoff in the initiating systems of VESF. In 1990, Weickert presented the results of an experimental investigation on cluster EFP warheads for the defeat of soft targets. The findings show that EFPs form properly in a cluster and the radial dispersion of EFPs can be changed by adjusting the number and distance of liners. Nevertheless, the literature review clearly reveals that the investigation on the design and testing of MEFP warheads at a certain standoff is limited and inconsistent. In particular, reports regarding the spatial dispersion patterns and penetration properties at different standoffs of MEFP are very few. Making comparisons or referencing the results from different investigations is also difficult because various MEFP warhead structures are involved, such as liner structures [Richard et al., 2005], charge structures [Richard et al., 2001; Blachel and Weimann,1999], and initiation methods [Blachel and Weimann,1999]. In conclusion, the findings about MEFP warheads are incomplete, without academic rigor and a greatly reduced credible degree of results. Therefore, studying the spatial dispersion patterns and penetration properties of the whole process of MEFP formation is crucial.

In the present study, a new integral MEFP warhead consisting of an integral explosive and seven hemispherical liners was designed. The results of a numerical study on the formation and penetration properties of MEFP combined with an experimental study on the penetration properties of MEFP at different standoffs were discussed.

2 DESIGN AND PARAMETERS OF MEFP WARHEAD

2.1 Design of MEFP Warhead

An integral-type MEFP warhead with seven liners was fabricated. The warhead structure comprised seven sub-liners (hemispherical liner), a booster, and an explosive (Figure 1). The seven sub-liners are located equally in the charge: one is located at the center and the rest are placed around it. The booster is initiated at the center of the back of the central liner, and one-point initiation method is adopted. Figure 2 shows a photograph of the MEFP charge. In the following discussion, we refer MEFP to the integral MEFP. The explosive is a cylinder of radius R_0 with seven round holes, which are used to install sub-liners and match the size of these sub-liners well. As shown in Section III of Figure 1, the explosive radius R_0 is expressed by

$$R_0 = L + D + d + \frac{D}{2} \tag{1}$$

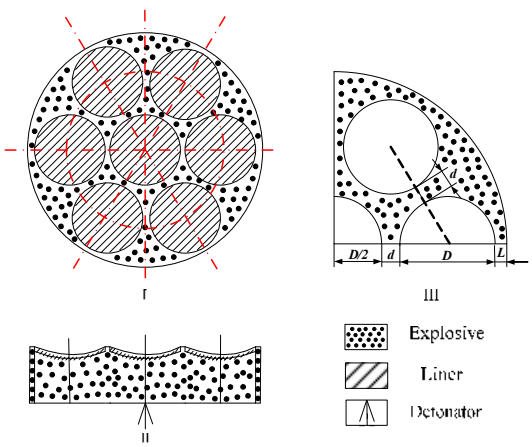

Figure 1: Configuration of MEFP charge.

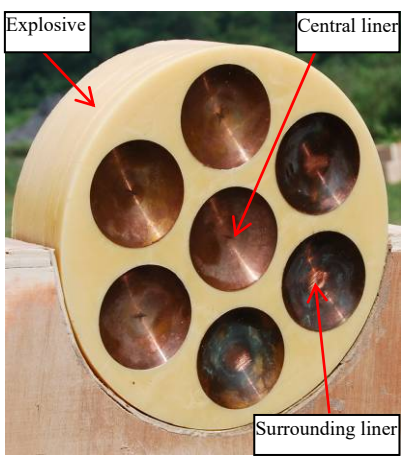

Figure 2: Photograph of MEFP charge.

In Eq. (1), L is the minimum distance from cylindrical hole surface to explosive cylinder surrounding surface; D is the diameter of round holes equal to the caliber of the liner; and d is the minimum distance between each cylindrical hole surface, namely, the space between neighboring sub-liners.

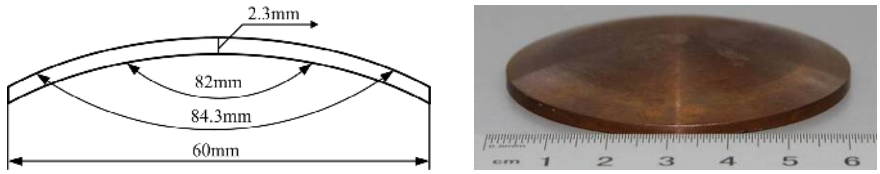

Figure 3: Structure of the liner.

The materials of MEFP charge and basic parameters dimension of liner are shown as follows:

(1) *Explosive*: The high explosive is Comp B with a nominal density of 1.717 g/cm^3 and a detonation velocity of 7980 m/s. The total weight of the explosive is 3737g. [Zhao et al., 2013].

(2) *Liner*: A hemispherical pattern liner was imparted into produce the individual penetrators. The diameter of the charge liner is 60 mm. Outer and inner curvature radius of liner (shown in Figure 3) is 82mm and 84.3mm, respectively. Considering the cost efficiency, we choose oxygen-free high-conductivity copper (OFHC) liner material with tensile strength of 35-45% and ductility of 45% [Zhao et al., 2015]. The liner weighs 60.3 g.

2.2 Definition of MEFP Divergence Angle and Damage Area

To facilitate analysis, the maximum divergence angle $a_{\max}$ and damage area S_x are used to measure and describe the radial dispersion of MEFP at different standoffs. A spatial rectangular coordinate system ($\vec{x}$ $\vec{y}$ $\vec{z}$) is established along the charge. A coordinate origin (0, 0, 0) is selected at the top central of the charge. Figure 4 displays a sketch map of the divergence angle and damage area. Divergence angle a indicates that the radial spray of MEFP can be expressed by

$$\alpha = arctg\frac{r}{z} \tag{2}$$

In Eq. (2), standoff z is the distance from the central of the MEFP warhead to the target plate; and r is the radial dispersion of penetrators, which could be determined by Eq. (3)

$$r = r_0 + V_r\, t \tag{3}$$

In the equation, r_0 is the distance between the central liner and the surrounding liner, r_0 = 0.07m; V_r is the radial velocity of surrounding penetrators; t is the time before the penetrator hits the target and can be determined by the following equation:

$$t = \frac{z}{V_x} \tag{4}$$

In the equation, V_x is the axial velocity of surrounding penetrator, so the divergence angle a is determined by Eqs. (2)–(4).

As shown in section A-A' of Figure 4, the sketch map of the damage area is expressed by S_z:

$$S_z = \pi r^2 \tag{5}$$

Damage area S_z is determined by Eqs. (3)–(5).

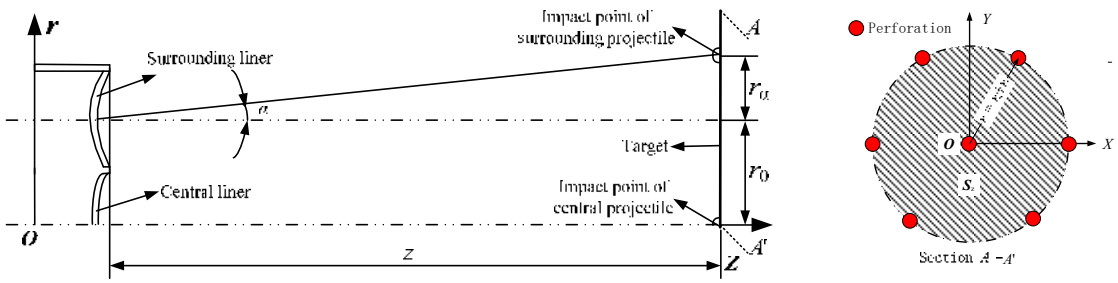

Figure 4: Sketch map of the divergence angle and the damage area.

3 NUMERICAL SIMULATION MODEL AND PARAMETERS OF MATERIALS

3.1 Establishment of the Simulation Model

Numerical simulation is carried out using three-dimensional (3D) dynamic finite element program of LS-DYNA in order to study the formation and dispersion patterns of MEFP. The simulation models of the MEFP warhead and the target are presented in Figure 5.

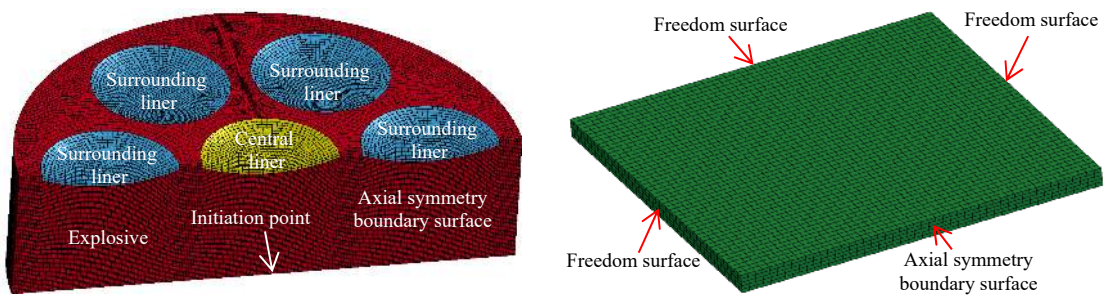

(*a*) MEFP warhead (*b*) Target

Figure 5: Simulation model of MEFP warhead and target (1/2 model).

Due to symmetry, modeling 1/2 of the geometry is necessary to simplify the analysis and reduce the computational cost. *BOUNDARY_SPC_SET [Hallquist,1997] is used in the simulation model to restrict elements movement in the symmetrical boundaries. The symmetrical inhibit condition is added to the symmetrical surface of the model to restrict the node's displacement and rotation degrees of freedom. Contact may occur along the surfaces of a single body undergoing large deformation, between two or more deformable bodies, or between a deformable body and a rigid barrier. Sliding interface with friction and separation approach is used to model the impact event between the penetrator and the target plate. The explosive, liner, and steel target are meshed with Lagrangian algorithm. *CONTACT_SLIDING_ONLY_PENALTY [Hallquist,1997] is used to model the impact between the dynamite and the shaped charge liner. The contact keyword between the formed penetrators and the target plate is changed to *CONTACT_ERODING_ SURFACE_TO_SURFACE. A large

number of numerical calculation results can prove that detonation products at about 30 μs will no longer affect the characteristic parameters of MEFP after the explosive is detonated; therefore, the explosive was deleted at 30 μs in the numerical calculation[Li et al., 2010].

3.2 Material Constitutive Models and Parameters

3.2.1 Material Model for High Explosive

High explosives (Comp B) are typically modeled by using the Jones-Wilkins-Lee (*JWL*) EOS, which models the pressure generated by chemical energy in an explosion. It can be written in the form

$$p = A_1\left(1-\frac{\omega}{R_1 v}\right)e^{-R_1 v} + B_1\left(1-\frac{\omega}{R_2 v}\right)e^{-R_2 v} + \frac{\omega e}{v} \tag{6}$$

where p is the hydrostatic pressure; v is the specific volume, e is internal specific energy. The values of constants A_1, R_1, B_2, R_2, ω for many common explosives have been determined from dynamic experiments.

3.2.2 Material Model for OFHC and #45 Steel

To be able to describe the various phenomena taking place during contact explosion, it is necessary to characterize the behavior of materials under explosion-generated high strain rate loading conditions. Liners and target are both modeled by the Johnson -Cook (*J-C*) material model [Johnson and Cook,1983], which is suitable to model the strength behavior of materials subjected to large strains, high strain rates and high temperatures. The model defines the yield stress σ_y as

$$\sigma_y = \left[A + B\left(\bar{\varepsilon}^{p}\right)^{n}\right]\left[1 + C\ln\dot{\varepsilon}^{*}\right]\left[1-\left(T^{*}\right)^{m}\right] \tag{7}$$

where A, B, C, n and m are the material parameters determined by experiments. $\bar{\varepsilon}^{p}$ is the equivalent plastic strain, $\dot{\varepsilon}^{*} = \dot{\varepsilon}_p / \dot{\varepsilon}_0$ is the dimensionless effective strain rate at a reference strain rate $\dot{\varepsilon}_0 = 1 s^{-1}$. T^{*} is the homologous temperature which is defined by $T^{*} = \left(T - T_{\text{room}}\right)/\left(T_{\text{melt}} - T_{\text{room}}\right)$, where T is the current temperature, T_{room} and T_{melt} are the room and melting temperatures, respectively.

In the fracture analysis, *J-C* fracture model [Dey et al., 2007] is used. The effective fracture strain is assumed to be the function of strain rate, temperature and pressure in the form

$$\varepsilon_f = [D_1 + D_2 \exp D_3\sigma^{*}][1 + D_4 \ln\dot{\varepsilon}^{*}][1 + D_5 T^{*}] \tag{8}$$

Where σ^{*} is the dimensionless pressure-stress ratio defined as $\sigma^{*} = \sigma_m/\bar{\sigma}$ where σ_m is the mean stress normalised by the effective stress, $\bar{\sigma}$ is the effective stress, and D_1, D_2, D_3, D_4 and D_5 are the material parameters. Details of finite element modeling of Comp B, copper liner and target are described in Table 1 [Zhao et al., 2016; Li et al., 2010].

Comp B	ϱ (g/cm^3)	D (km/s)	P_{CJ} (GPa)	A_1 (GPa)	B_1 (GPa)	R_1	R_2	ω	E_0 (GPa)	V_0
	1.717	7.98	29.5	524.23	7.678	4.20	1.1	0.34	0.085	1.00
Copper	ϱ (g/cm^3)	G (GPa)	A (MPa)	B (MPa)	N	C	m	T_m	σ_s (GPa)	C (km/s)
	8.97	46.50	90	292	0.31	0.025	1.09	1356	0.09	3.94
	S_1	S_2	S_3	γ_0	a	E_0	V_0			
	1.49	0	0	2.02	0.47	0	1.0			
#45 steel	ϱ (g/cm^3)	G (GPa)	A (MPa)	B (MPa)	N	C	m	T_m	σ_s (GPa)	C (km/s)
	7.83	77.00	792	510	0.26	0.014	1.03	1793	0.09	4.569
	S_1	S_2	S_3	γ_0	a	E_0	V_0			
	1.49	0	0	2.17	0.46	0	1.0			

Table 1: Parameters of each material.

4 NUMERICAL STUDY ON THE FORMATION AND PENETRATION PROPERTIES OF MEFP

4.1 Formation Process and Dispersion Pattern of MEFP

For a point initiated MEFP charge, detonation wave front will first have a normal impact to the central liner and maximum momentum will be given to this liner. The liners positioned in outer will be distorted because they are subjected to unsymmetrical detonation pressure [Pappu and Murr, 2002; Wang and Feng, 1998]. In fact, materials will fail if the stress suffered as penetrator stretching exceeds the material yield limit. Surrounding penetrators obtain a radial velocity during detonation wave have a oblique impact to the surrounding liners. All surrounding penetrators travel in a radial divergence toward the target with same velocity. Table 2 demonstrates the formation process of MEFP at different standoffs. Six penetrators surround a large aspect ratio of EFP in the radial distribution have been formed at last. As the standoff increased, the damage area of MEFP increased rapidly and the deformation of surrounding penetrators appeared.

Figure 6 gives trajectory curves of central penetrator and surrounding penetrators. An EFP formed by central liner moves along a straight line because detonation wave have a normal impact to the surface of central liner and six surrounding penetrators scattered around EFP. Figure 7 displays velocity of central penetrator and surrounding penetrator. The speed difference between central EFP and surrounding penetrator is small in this structure design. Velocity of all penetrators is about 2500m/s. The respective divergence angle and damage area of MEFP during the formation process are presented in Figures 8 and 9. The radial divergence angle is numerically predicted to be 7.8°.

The curve shape of S-t is approximate with a parabola. So a parabolic fitting process($y=ax^2+bx+c$) was carried out for the damage area versus time based on Parabola model. An equation related to damage area and time was obtained,

$$S=\begin{cases} 0.015m^2, & s\le 0.015m^2 \\ 0.31t^2-0.036t+0.011, & s>0.015m^2 \end{cases} \tag{9}$$

Unit is s, m. Coefficient of determination (R^2) is 0.99. The initial damage area regarded as the coverage of surrounding liners, $S(t=0)=0.015\text{m}^2$.

z =0.10m	z =0.20m	z =0.30m	z =0.45m
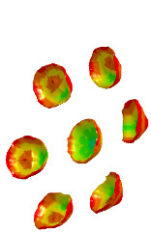	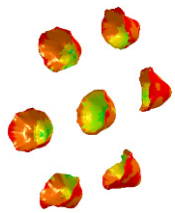	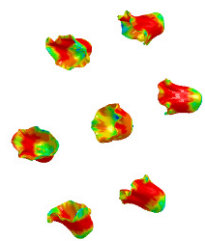	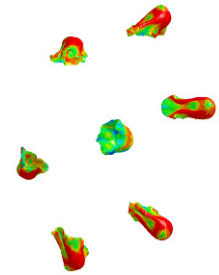
z =0.6m	z =0.8m	z =1.2m	z =1.5m
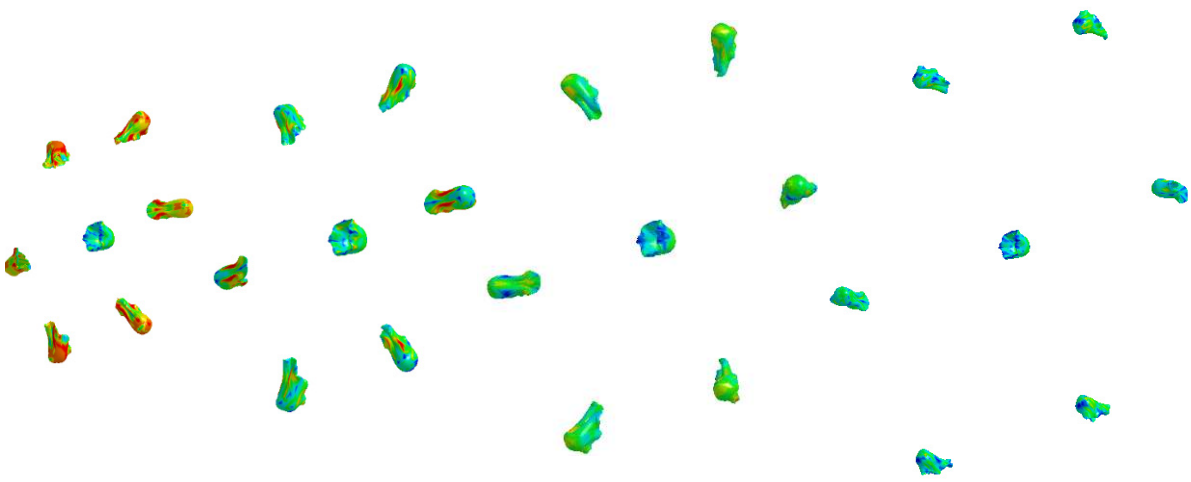			

Table 2: Formation pattern of MEFP at different standoffs.

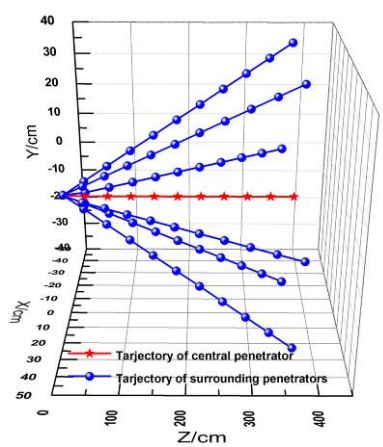

Figure 6: Trajectory of central penetrator and surrounding penetrators.

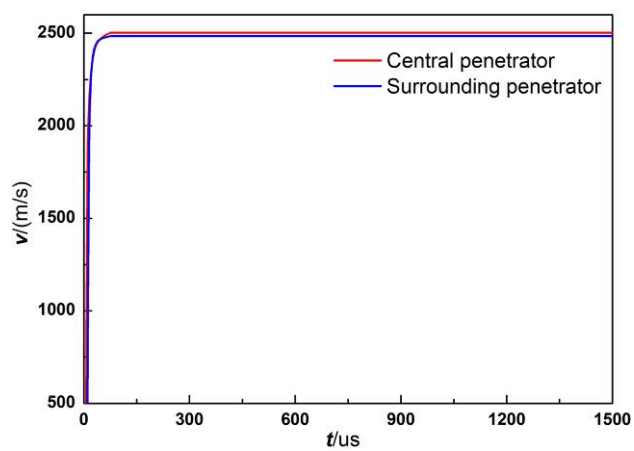

Figure 7: Velocity of central penetrator and surrounding penetrator.

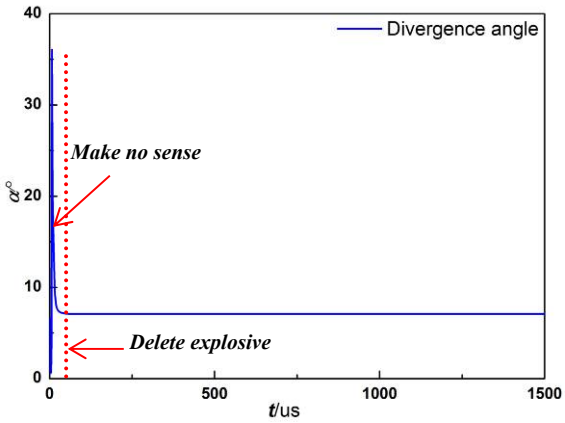

Figure 8: Divergence angle of MEFP.

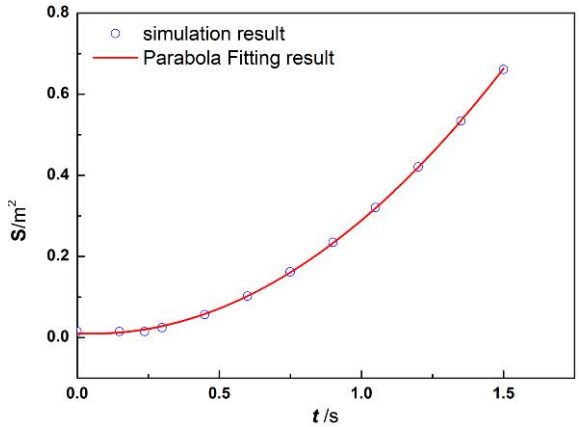

Figure 9: Damage area of MEFP.

Numerical results successfully presented the formation process of MEFP: central liner can form an EFP has a good aerodynamic shape and surrounding liner can form a distorted EFP at different standoffs. We also obtained parameters of MEFP by numerical calculation.

4.2 Penetration Process and Perforations Dispersion Pattern of MEFP

Further research on the penetration patterns and properties of MEFP has been carried out to obtain the penetration properties of MEFP at different standoffs. The penetration results of MEFP against #45 steel targets are given in Table 3.

According to the numerical simulation results, a group of penetrators consisting of a central penetrator surrounded by six distorted penetrators is formed during the formation process of MEFP. Both central penetrator and surrounding penetrators can effectively break down the #45 steel target with a thickness of 1.5cm. The spatial dispersion pattern of MEFP has been studied based on the perforation information on the steel targets at different standoffs.

Observations on targets and measurements of damage area in simulation, a nonlinear fitting process was also carried out for the perforations based on Poly model. Figure 10 displays nonlinear fitting picture of perforations on the targets. Model of spatially perforations is obtained, as shown in Eq. (10).

$$z = z_0 + ax + by + cx^2 + dy^2 + exy(z \geq 0) \tag{10}$$

z_0=-0.062, c=d=23.7, a= b= e ≈0. Unit is m. Coefficient of determination (R^2) is 0.99. Eq. (10) can also be described by

$$z = z_0 + k(x^2 + y^2)(z \geq 0) \tag{11}$$

z_0=-0.062, k=23.7.

z/m	Isometric view of MEFP and target before impact	Isometric view of MEFP and target after impact
0.45	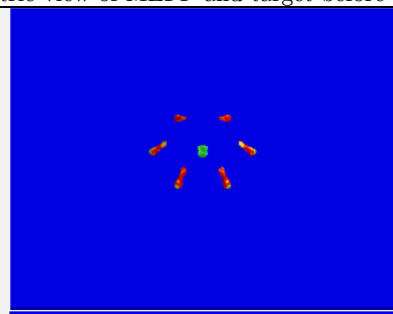	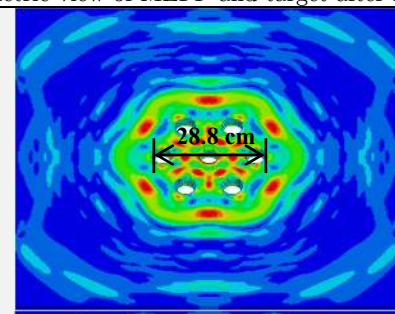
0.6	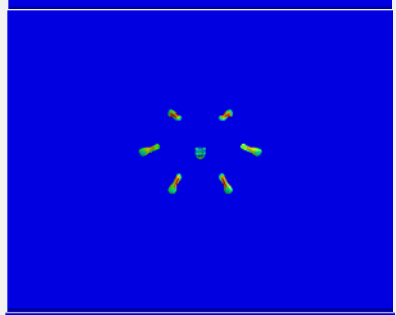	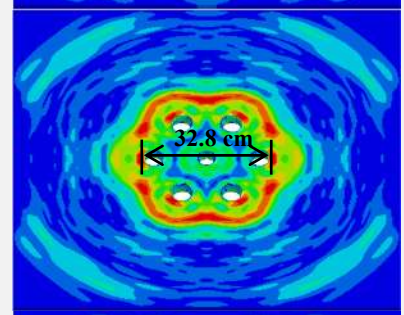
0.8	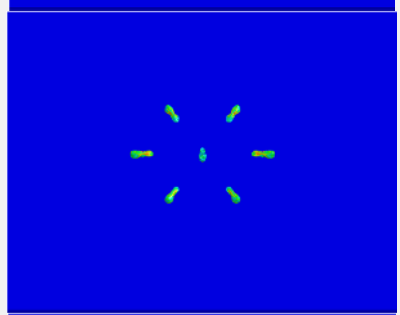	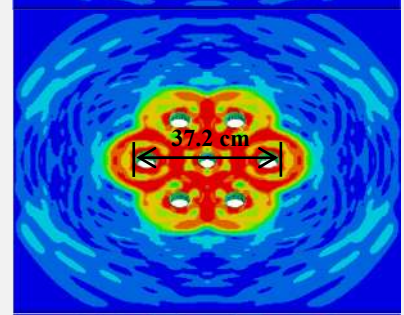
1.2	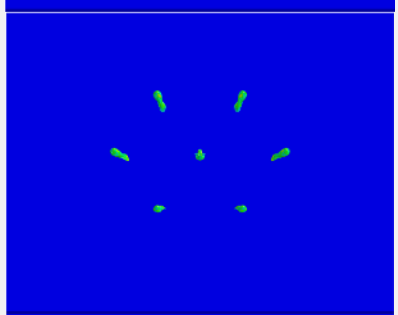	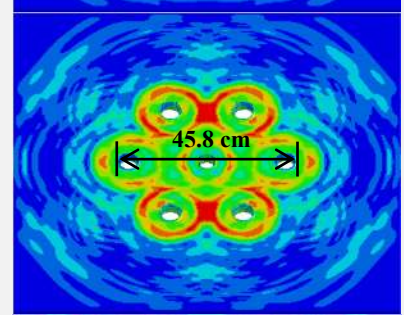
1.5	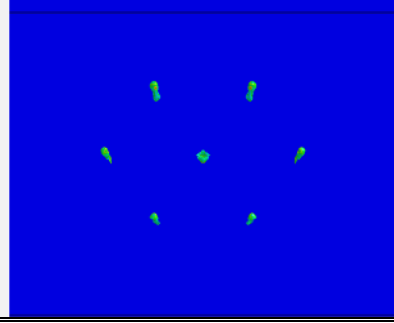	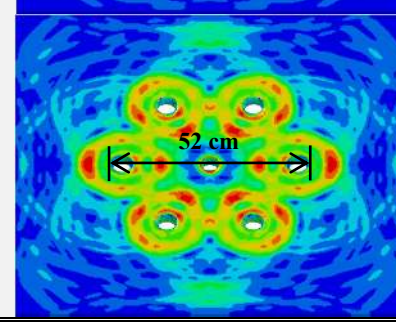

Table 3: Penetration results of MEFP against 45# steel targets at different standoffs (1/2 model).

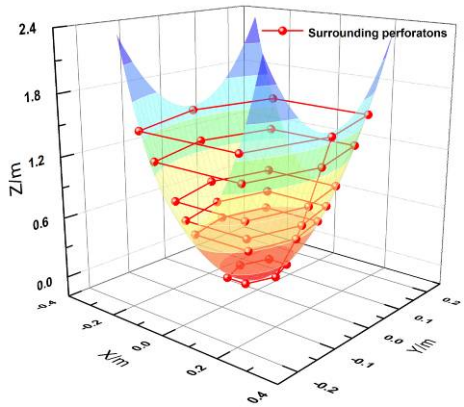

Figure 10: Track of MEFP spatial movement.

MEFP warhead can form a fragments group contains 7 penetrators which has the ability to breakdown a 1.5cm thickness steel target. A nonlinear fitting process obtains laws of spatially perforations. It provided an effectively method to predict perforations spatial distribution model.

5 EXPERIMENTAL INVESTIGATIONS

5.1 Experimental Setup and Program

Experiments on an MEFP warhead against a #45 steel target were carried out to verify the penetration properties and spread pattern of the MEFP. Two #45 steel targets (front target and rear target) with a dimension of 160cm × 160cm × 1.5cm were positioned in front of the MEFP warhead at different standoffs. Figure 11 illustrates the schematic sketch of the experiment conducted on a MEFP warhead against a #45 steel target. The MEFP warhead was placed on a special wooden support frame after the front and rear targets were set up. The central of the MEFP warhead and the front target were arranged in the same horizontal plane by adjusting the aiming sight and level gauges.

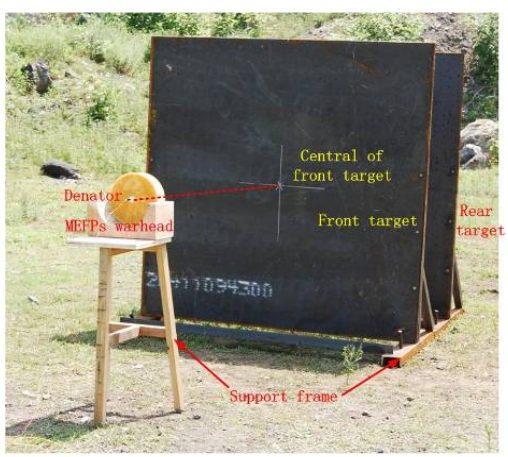

Figure 11: Experimental setup of MEFP warhead against 45# steel target.

Three kinds of projects were designed according to varies of standoffs in order to verify the penetration ability of MEFP and the spray state of sub-penetrators. Standoffs were set 0.45m, 0.60m and 1.2m, respectively.

5.2 Results and Discussion

Perforations on witness targets at different standoffs are present in Table 4. Seven perforations were recorded on the target when standoff was at 0.45 m. This result means seven penetrators were formed at this movement. The #45 steel target was subjected to normal impact by the central EFP and oblique impact by the surrounding penetrators. Owing to the geometric structure design, material selection, and machining techniques of the liner and explosive, surrounding perforations in the steel target were not completely symmetrical in the experiment. Especially, tails of some surrounding penetrators broken when the standoff reaches 1.2m.

z /m	0.45	0.60	1.20
Front view	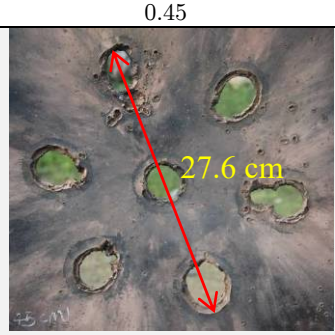	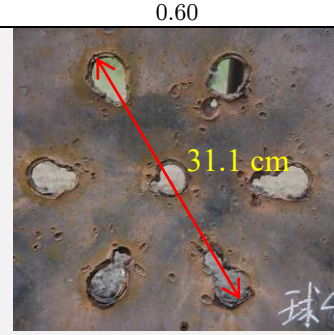	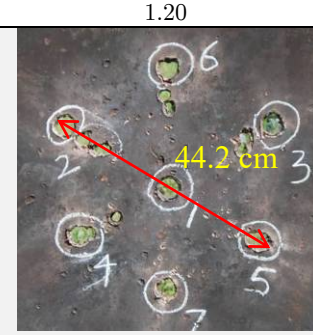
Rear view			

Table 4: Perforations on the witness target at different standoffs.

Research on the statistical information of perforation on the target indicates that the divergence angle and damage area of integral MEFP can be derived by Eq. (2) and (5), as shown in Figures 12 and 13. Figure 12 displays divergence angle of MEFP. With the increase of standoff, the divergence angle is gradually reduced and it will remains at about 7°. The damage area of MEFP is presented in Figure 13. Maximum damage area is $0.16m^2$ at standoff up to 1.2m. Besides, numerical results is bigger than experimental results, mainly due to the numerical calculation process did not consider air resistance and some other external factors.

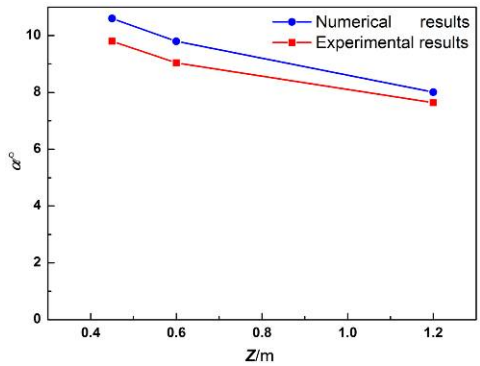

Figure 12: Comparison of simulation with experiment for divergence angles.

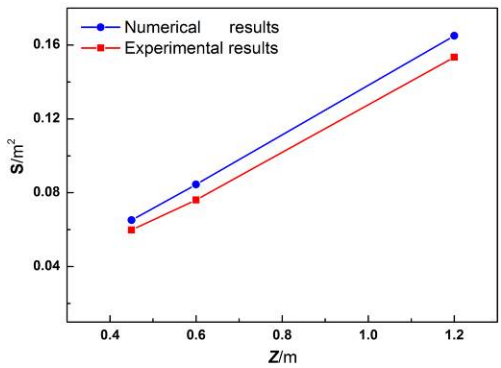

Figure 13: Comparison of simulation with experiment for damage area.

Experimental results show that a group of penetrators consisting of a central penetrator surrounded by 6 penetrators is formed during the formation process of MEFP and moves in the direction of aiming position. It can effectively defeat targets, such as low-flying aircraft, attacking missiles, and light targets, at an appropriate standoff. The experimental results are in agreement with the simulation results.

6 CONCLUSIONS

We design a new MEFP warhead with seven hemispherical liners which can form 7 penetrators at different standoffs. The whole process of formation and penetration of MEFP is simulated by a 3D coupled hydrocode of LS-DYNA. Simulation results of MEFP formation process had successfully explained distribution mode of perforations on the witness targets at different standoffs.

Once initiated, the maximum divergence angle of the surrounding penetrator is 7.8°, and the damage area can reach $0.16m^2$ at 1.2 m. The damage area improves rapidly when the standoff increases and we also offered a method to forecast damage area of MEFP at different standoffs. Space curve equation based on the Poly model is established to describe the perforations distribution on the witness target of MEFP. The equation can be expressed by

$$z = z_0 + k(x^2 + y^2)(z \geq 0)$$

Fitting results can able to meet the requirements of engineering applications. So it provides a way to predict the perforation dispersion patterns of MEFP.

Compared with conventional EFP, a group of penetrators consisting of a central penetrator surrounded by 6 penetrators is formed during the formation process of MEFP and moves in the direction of aiming position. It can effectively breakdown a 1.5 cm 45# steel target at different standoffs in experiment.

Acknowledgments

This research was supported by the Advanced Research of PLA University of Science and Technology (201417) and Science Foundation of College of Filed Engineering (No. 2015-7).

References

Bill G, Campbell III, Phil G. C et al, (1991). Advances in Multiple Explosively Formed Penetrator Technology. Proceedings of the 41st Annual Bomb & Warhead Technical Meeting. San Diego California. May 15-16:207-220.

Blachel A. and Weimann K., (1999). Muti-EFP-Charge for Lightweight Armor Defeat. In. Proceedings of the 18th international symposium on ballistics, Sanantonio, Texas:15-19.

David B., Richard F., William Ng. et al, (2001). Dual mode warhead technology for future smart munitions. In. Proceedings of the 19th international symposium on ballistics, Interlaken, Switzerland: 679-684.

Dey S., Bϕrvik T., Hopperstad O.S., et al, (2007). On the influence of constitutive relation in projectile impact of steel plates, International Journal of Impact Engineering 34:464-486.

Hallquist J.O., (1997). LS-DYNA Theoretical Manual, Livermore Software Technology Corporation, Livermore, CA, USA.

Johnson C.R., Cook W.H., (1983). A constitutive model and data for metals subjected to large strain, high strain rates and high temperature. In. Proceedings of the 7th International Symposium on Ballistics, Hague, Netherlands:541-548.

Johnson G.R., Stryk R.A., (2006). Some considerations for 3D EFP computations. International Journal of Impact Engineering 32(10):1621-1634.

Kazuo S., Takenori O., (2013). Study of Water Entry of High-Speed Projectile. Procedia Engineering 58:232-239.

Li W.B., Wang X.M., Li W.B., (2010). The effect of annular multi-point initiation on the formation and penetration of an explosively formed penetrator. International Journal of Impact Engineering 37:414-424.

Long Y., Zhang Y.Y., Yu D.Q., et al, (2010). Forming process and effect of the factors on radial dispersion angle of fragments in a dual-mode warhead. Acta Armamcntarii 31:7-12.

Pappu S., Murr L.E., (2002). Hydrocode and microstructural analysis of explosively formed penetrators, Journal of materials science 37:233-248.

Richard F., (2000). Warhead Technology Advancements. Armaments for the Army Transformation Conference.June:19-21.

Richard F., Rockaway, William N.J., (1996). Selectable effects explosively formed penetrator warhead[P]. United States, 5540156, Jul.30.

Richard F., William Ng., Bernard R., et al, (2001). Multiple Explosively Formed Penetrator (MEFP) warhead technology development. In. Proceedings of the 19th international symposium on ballistics, Interlaken, Switzerland:563-568.

Richard F., William Ng., Steve Tang, et al, (2005). Multiple explosively formed penetrator (MEFP) warhead technologies for mine and improvised explosive device (IED) neutralization. In. Proceedings of the 22th international symposium on ballistics, Vancouver, BC Canada: 669-677.

Saroha R., Singh Y., Mahala V.K., (2010). Single point initiated multi-EFP warhead, In. Proceedings of the 25th international symposium on ballistics, Beijing, China: 1298-1302.

Wang H.F., Feng S.S., (1998). Theoretical Initial Shock Properties of Porous Materials Under Explosion Loads. Journal of Beijing Institute of Technology. 18(5): 634-637.

Weickert C.A., (1990). Explosively Formed Projectile Clusters For Defeat of Soft Target. In. Proceedings of the 12th international symposium on ballistics, Sanantonio, Tesas:465-475.

William Ng., (2002). Long Standoff Demolition Warheads for Armor. Masonry and Concrete Targets, Mines, Demolition and Non-Lethal Conference 4 June.

Wu J., Liu J.B. and Du Y.X., (2007). Experimental and numerical study on the flight and penetration properties of explosively-formed projectile. International Journal of Impact Engineering 34:1147-1162.

Zhang Y.Y., Long Y., Ji C. et al, (2012). Superposition effect of shock waves on formation of a grouped multiple explosive formed projectile. Journal of vibration and shock 31:56-60.

Zhao C. X., (2013). Technological researches on multiple explosive formed projectiles. PhD thesis, Nanjing: PLA University of Science and Technology.

Zhao C. X., Qian F., Xu J. G., Cao H. A., Ji C., Lu L., (2016). Effect of liner configuration parameters on formation of integral MEFP, Chinese journal of energetic materials 24(5):485-490.

Zhao C. X., Qian F., Zhang H. Z., Ji C., Lv Y., Xie Q. M., (2015). Influence of liner material on formation of multiple explosively formed projectiles warhead parameters. Advanced Materials Research 1096:37-41.

Zhao C.X., Long Y., YU D.Q., et al, (2013). Formation of incised multiple explosively-formed projectiles and their armor-piercing effect against steel target. Explosive and shock waves 33:186-193.

Zhou X., Long Y., YU D.Q., et al, (2006). Numerical simulation and effect analysis for radial dispersion of MEFP. Acta Armamcntarii 27:23-26.